ACS Catalysis

Research Article

pubs.acs.org/acscatalysis

# Insights into Hägg Iron-Carbide-Catalyzed Fischer–Tropsch Synthesis: Suppression of $CH_4$ Formation and Enhancement of C–C Coupling on $\chi$-$Fe_5C_2$ (510)

Thanh Hai Pham,[†] Yanying Qi,[‡] Jia Yang,[§] Xuezhi Duan,*[,†] Gang Qian,[†] Xinggui Zhou,[†] De Chen,[‡] and Weikang Yuan[†]

[†]State Key Laboratory of Chemical Engineering, East China University of Science and Technology, 130 Meilong Road, Shanghai 200237, China

[‡]Department of Chemical Engineering, Norwegian University of Science and Technology, N-7491 Trondheim, Norway

[§]SINTEF Materials and Chemistry, N-7463 Trondheim, Norway

Supporting Information

**ABSTRACT:** Probing the product selectivity of Fischer–Tropsch catalysts is of prime scientific and industrial importance—with the aim to upgrade products and meet various end-use applications. In this work, the mechanisms for $CH_4$ formation and $C_1$–$C_1$ coupling on a thermodynamically stable, terraced-like $\chi$-$Fe_5C_2$ (510) surface were studied by DFT calculations. It was found that this surface exhibits high effective barriers of $CH_4$ formation for the three cases (i.e., 3.66, 2.81, and 2.39 eV), indicating the unfavorable occurrence of $CH_4$ formation under FTS conditions. The C + CH and CH + CH are the most likely coupling pathways, which follow the carbide mechanism. Subsequently, the effective barrier difference between $CH_4$ formation and $C_1$–$C_1$ coupling was used as a descriptor to quantify FTS selectivity. A comparison of the selectivity between this surface and the reported FTS catalysts' surfaces was discussed in detail. More interestingly, this surface shows unexpectedly high $C_{2+}$ selectivity. This indicates that manipulating the crystal facet of $\chi$-$Fe_5C_2$ catalyst can effectively tune the FTS selectivity, which will open a new avenue for highly selective Fe-based FTS catalysts.

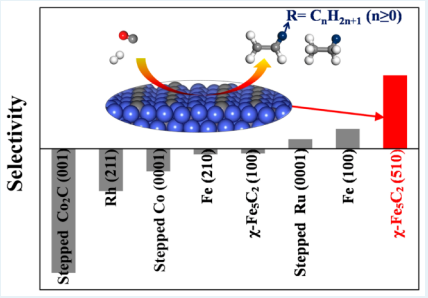


**KEYWORDS:** *$\chi$-$Fe_5C_2$ catalyst, Fischer–Tropsch synthesis selectivity, $CH_4$ formation, C–C coupling, carbide mechanism*

## 1. INTRODUCTION

Conversion of coal-, biomass-, or natural gas-derived syngas via Fischer–Tropsch synthesis (FTS) has recently gained a renewed interest as a nonpetroleum, promising alternative route to produce clean fuels and value-added chemicals (e.g., lower olefins).[1−6] Selectivity is one of the most important issues in an intricate FTS network including many surface intermediates and elementary steps.[7−11] Taking into account that methane is the least desired product,[12] mechanistic studies on how to reduce its selectivity or even suppress its formation are highly encouraged for designing and optimizing FTS catalysts.

FTS selectivity highly depends on the reaction conditions and the catalyst types, and commercial FTS catalysts are based on Fe or Co with the low cost and high selectivity of hydrocarbons.[1−12] Fe catalysts are more attractive in two aspects compared to Co catalysts:[13,14] (i) converting CO-rich and contaminant-containing syngas from coal or biomass feedstock because of the higher activity of water–gas shift and resistance to contaminants; (ii) catalyzing high-temperature FTS owing to the lower methanation activity and higher catalytic efficiency. Up to now, many efforts, including selecting supports, adjusting pretreatment conditions, optimizing catalyst particle sizes, and adding promoters, have been made to lower $CH_4$ selectivity and raise $C_{2+}$ selectivity of Fe-based catalysts.[4,5,7,10,13] Furthermore, some experimental and theoretical evidence has prompted researchers to use iron carbides, especially Hägg iron carbide ($\chi$-$Fe_5C_2$), as the active phases among various iron species from the complex phase transformation of working Fe FTS catalysts.[15−19] Recently, Hu and co-workers have used the effective barrier difference between $CH_4$ formation and $C_1$–$C_1$ coupling ($\Delta E_{eff}$, the derivation details in Supporting Information), proposed in their pioneering work,[20] as a descriptor to analyze FTS selectivity on the Fe-terminated $\chi$-$Fe_5C_2$ (100) surface.[17]

It is worth mentioning that unlike metallic surfaces, some high Miller index surfaces of $\chi$-$Fe_5C_2$ especially (510), detected by XRD and HRTEM,[19,21,22] exhibit lower surface energies and thus have the larger percentages among the exposed crystal facets.[23] Recently, DFT calculations of CO activation on $\chi$-$Fe_5C_2$ (monoclinic crystal structure and "a" being the highest among the lattice parameters) surfaces showed that the

Received: October 28, 2014
Revised: February 17, 2015
Published: February 25, 2015




DOI: 10.1021/cs501668g
ACS Catal. 2015, 5, 2203−2208

terraced-like (510) surface prefers the direct CO dissociation route,[23] whereas the stepped-like (010) and (001) surfaces prefer the H-assisted CO dissociation route,[16,24] and the stepped-like (100) surface prefers both direct and H-assisted CO dissociation routes.[25] Additionally, the (510) surface is suggested as the active facet of FTS because the direct CO dissociation route generally corresponds to high FTS activity.[23,26] Therefore, as a consecutive effort, probing FTS selectivity on the (510) surface is highly desirable.

The purpose of this study is to investigate FTS selectivity on a thermodynamically stable, terraced-like $\chi$-$Fe_5C_2$ (510) surface by periodic spin-polarized DFT calculations. All possible reaction pathways including carbide and CO insertion mechanisms for $CH_4$ formation and $C_1$−$C_1$ coupling were considered and analyzed with the objective to identify the active sites and reaction mechanisms. Subsequently, the effective barrier difference between $CH_4$ formation and $C_1$−$C_1$ coupling ($\Delta E_{eff}$) was employed as a descriptor to evaluate the FTS selectivity. Finally, the selectivity between the $\chi$-$Fe_5C_2$ (510) surface and the reported FTS catalysts surfaces was compared and discussed in detail, and then some insights were proposed. This might guide the design of highly selective Fe-based FTS catalysts with the suppression of $CH_4$ formation and enhancement of C−C coupling.

## 2. COMPUTATIONAL DETAILS

**2.1. Methods.** All of the periodic spin-polarized DFT calculations were performed using the Vienna ab initio simulation package (VASP).[27−30] The interactions between ion cores and valence electrons were described by the projector augmented wave (PAW) method,[31] and the exchange−correlation functional was GGA-PBE.[32,33] The solution of the Kohn−Sham equations was expanded in a plane wave basis set with a cutoff energy of 400 eV. The Brillouin zone sampling was performed using a Monkhorst−Pack grid,[34] and electronic occupancies were determined in light of a Methfessel−Paxton scheme with an energy smearing of 0.2 eV.[35] The Dimer method[36] was used to determine the transition states of the elementary steps of $CH_4$ formation and C−C coupling reactions. In all the calculations, a force-based conjugated-gradient method was used to optimize the geometries.[37] Saddle points and minima were considered to be converged when the maximum force in each degree of freedom was less than 0.03 eV/Å. Furthermore, the vibrational frequencies were analyzed to evaluate if a stationary point is a minimum state with no imaginary frequencies or a transition state with only one imaginary frequency, and zero-point energy (ZPE) was considered for all the calculated energy data.

**2.2. $\chi$-$Fe_5C_2$ (510) Surface Models.** Surface reactions were calculated on p(1 × 1) supercell slab with four-layered iron and eight-layered carbon. The Monkhorst−Pack mesh of 4 × 2 × 1 k-point sampling in the surface Brillouin zone was used. The bottom two-layered iron and four-layered carbon were fixed, whereas the top two-layered iron, four-layered carbon, and adsorbates were relaxed. The vacuum spacing between slabs was around 10 Å. The top and side views of the studied $\chi$-$Fe_5C_2$ (510) surface were illustrated in Figure 1. Moreover, Table S1 and Table S2 summarize the influences of the vacuum thickness and supercell size for the C + CH → CCH and $CH_2$ + $CH_3$ → $CH_2CH_3$ reactions, respectively. This could validate the applicability of our model.

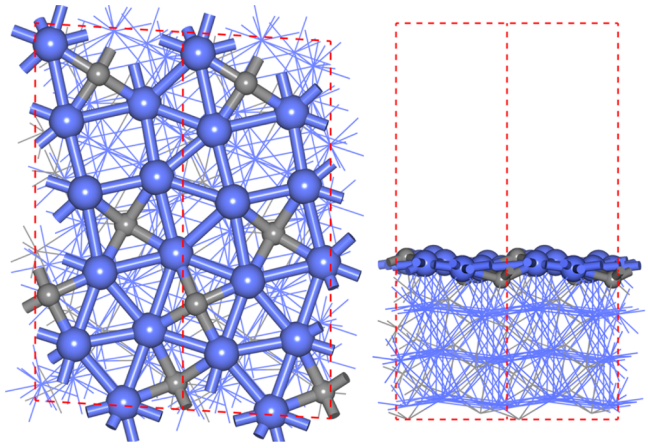

**Figure 1.** Top (left) and side (right) views of $\chi$-$Fe_5C_2$ (510) surface (Blue: Fe atoms; gray: C atoms). Dashed box shows the unit cell of p(1 × 1).

## 3. RESULTS AND DISCUSSION

**3.1. $CH_4$ Formation Mechanism.** When exposing Hägg iron carbide to syngas, two kinds of mechanisms for $CH_4$ formation primarily occur by means of (i) stepwise hydrogenation of the surface C atom and (ii) direct or H-assisted dissociation of the adsorbed CO and subsequent stepwise hydrogenation. Our previous studies show that on terraced-like $\chi$-$Fe_5C_2$ (510) surface, direct CO dissociation is the preferred activation pathway.[23] Therefore, there are three possibilities for $CH_4$ formation: **Case 1**, stepwise hydrogenation of the surface C atom on the clean surface; **Case 2**, stepwise hydrogenation of the surface C atom on the dissociated C adsorbed surface; **Case 3**, stepwise hydrogenation of the dissociated C atom on the dissociated C adsorbed surface.

Let us first consider $CH_4$ formation mechanism of **Case 1**, because of the surface C atom occupied site previously suggested as the active sites for $CH_4$ formation.[16] The optimized structures of the chemisorbed $C_1$ species and transition states (TSs) of elementary steps are shown in Figure S1 and Figure 2, respectively. As we can see, the most stable adsorption sites for C, CH, and $CH_2$ are the 4-fold site, although the bridge site is favored by $CH_3$; at the TSs, C, CH, and $CH_2$ adsorb at the 4-fold site, and $CH_3$ adsorbs at the top site. The geometries are very similar to those on the Fe (100) surface.[38,39]

Figure 3 illustrates the energy profile of $CH_4$ formation in **Case 1**. It is clearly seen that the total energy of the TSs increases along the hydrogenation coordinate (i.e., the last step has the highest TS energy). Moreover, $CH_3$ compared to C, CH, and $CH_2$ species is not thermodynamically stable and thus has low site coverage. It can be concluded that $CH_3$ hydrogenation is the slowest. This would suggest that this step is the rate-determining step of $CH_4$ formation and the preceding hydrogenation steps reach quasi-equilibrium. Therefore, the effective barrier of $CH_4$ formation ($E_{eff,CH4}$, the derivation details in Supporting Information[17,20,40,41]) was used as a descriptor to evaluate the reaction rate of $CH_4$ formation. Unexpectedly, the $E_{eff,CH4}$ of **Case 1** is up to 3.66 eV, indicating that the $CH_4$ formation is very difficult to occur under FTS conditions.

The $CH_4$ formation mechanisms of **Case 2** and **Case 3** were further studied. The chemisorption of $C_1$ species and the TSs of elementary steps were calculated, and the corresponding energy



DOI: 10.1021/cs501668g
ACS Catal. 2015, 5, 2203−2208

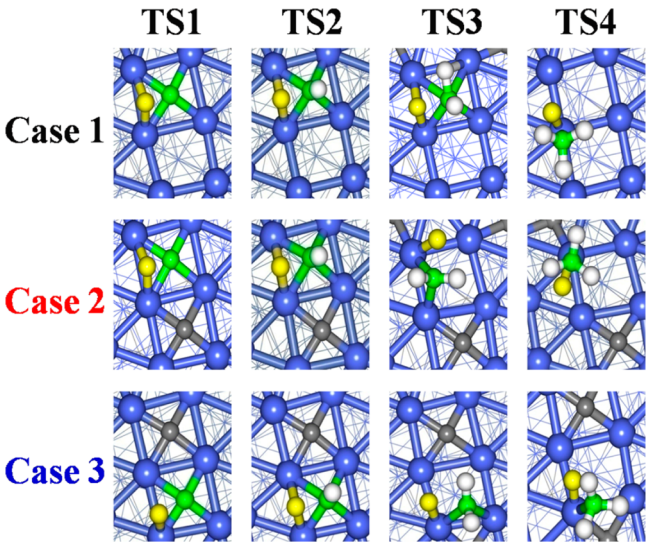


**Figure 2.** Structures of the TSs of elementary steps involved in the methanation reactions in the three cases. Blue: Fe atoms; gray: C atoms; green: C atoms involved in reactions; white: H atoms; yellow: H atoms involved in reactions.

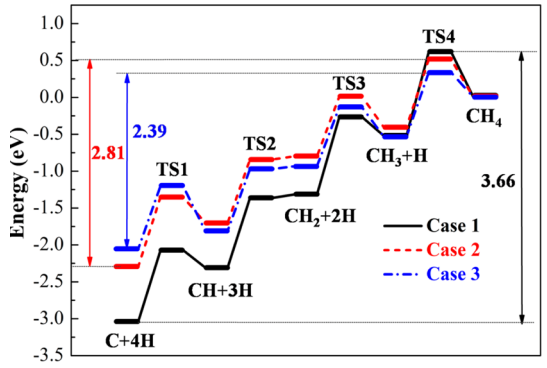


**Figure 3.** Energy profiles of $CH_4$ formation in the three cases. The corresponding effective barriers were also presented.

profiles were plotted. It can be clearly seen that these two cases are very similar to **Case 1** regardless of the optimized structures of chemisorbed $C_1$ species (Figure S1) and TSs (Figure 2) or the nature of stepwise-increasing energy profiles (Figure 3). However, the chemisorption energies of H and $C_1$ species in these two cases are different from those in **Case 1** (Table S3). Moreover, the C−H distances ($d_{C-H}$) at the TSs and the calculated reaction barriers of the elementary steps in the three cases are given in Table 1. It is apparently observed that $d_{C-H}$ of the latter three elementary steps follows the order of **Case 1** < **Case 2** < **Case 3**, while $E_a$ of each elementary step follows the trend of **Case 1** > **Case 2** > **Case 3**.

It can be also seen in Figure 3 that the effective barriers of $CH_4$ formation in **Case 2** and **Case 3** are 2.81 and 2.39 eV, respectively. They are lower than the $E_{eff,CH4}$ in **Case 1** (i.e., 3.66 eV). Considering the similar geometric structures in the three cases, the difference in $E_{eff,CH4}$ is most likely due to the difference in the electronic properties of surface Fe atoms. As shown in Figure S2, the average d-band centers ($\varepsilon_d$) of surface Fe atoms in the three cases follow the order of **Case 1** > **Case 2** > **Case 3.** It is reported that the site with d-band center far from the Fermi energy is more active for hydrogenation.[16] This would provide a rational interpretation for the **Case 3** with the lowest barrier. Furthermore, Figure S3 exhibits a linear relationship between $E_{eff,CH4}$ and $\varepsilon_d$ in the three cases. This demonstrates that the difference in $E_{eff,CH4}$ in the three cases is mainly ascribed to the difference in the electronic properties of surface Fe atoms. This is consistent with previous results (i.e., a linear relationship between the effective barrier of $CH_4$ formation on different iron carbides and the d-band center of surface Fe atom).[16]

On the basis of the above results, **Case 3** is found to have the lowest effective barrier of $CH_4$ formation. However, it is much higher than that of the stepped-like $\chi$-$Fe_5C_2$ (010) surface (1.54 eV),[16] where the similar computational methods were employed. This suggests that on the one hand, the terraced-like $\chi$-$Fe_5C_2$ (510) surface is less active toward $CH_4$ formation; on the other hand, $CH_4$ formation is highly sensitive to $\chi$-$Fe_5C_2$ crystal facet.

**3.2. $C_1$−$C_1$ Coupling Mechanism.** To probe FTS selectivity on $\chi$-$Fe_5C_2$ (510) surface, $C_1$−$C_1$ coupling reactions were further studied. As shown in Table 2, 10 kinds of $C_1$−$C_1$ coupling reactions between $CH_i$ ($i$ = 0−3) derived from the surface C and $CH_j$ ($j$ = 0−3) from the dissociated C in terms of the carbide mechanism were first considered. The optimized structures of TSs are listed in Figure S4. At the TSs, the most stable adsorption sites of C and CH, $CH_2$ as well as $CH_3$ are 4-fold site, 3-fold or bridge site and top site, respectively, which are very similar to those on Fe (100) surface.[42,43] Moreover, the C−C distances at the TSs and the reaction barriers and reaction energies of $CH_i$ + $CH_j$ are also summarized in Table 2. Subsequently, the effective barrier of $CH_i$ + $CH_j$ reactions ($E_{eff,CH_i-CH_j}$, the derivation details in Supporting Information[17,20,40,41]) was used as a descriptor to evaluate the reaction rate of $C_1$−$C_1$ coupling. It can be seen in Table 2 that the C + C coupling reaction among the $CH_i$ + $CH_j$ ones has the largest reaction barrier, and the resultant C−C product is very unstable. More interestingly, the C + CH and CH + CH coupling reactions have relatively lower individual reaction barrier and effective barrier than other $C_1$−$C_1$ coupling

**Table 1. C−H Distances ($d_{C-H}$) at the TSs and Reaction Barriers ($E_a$) of Elementary Steps Involved in $CH_4$ Formation in the Three Cases[a]**

| | $d_{C-H}$ (Å) | | | $E_a$ (eV) | | |
|---|---|---|---|---|---|---|
| reactions | Case 1 | Case 2 | Case 3 | Case 1 | Case 2 | Case 3 |
| C + H→CH | 1.456 | 1.444 | 1.550 | 0.97 (1.01) | 0.95 (0.99) | 0.86 (0.93) |
| CH + H→$CH_2$ | 1.393 | 1.412 | 1.437 | 0.94 (0.95) | 0.86 (0.87) | 0.84 (0.87) |
| $CH_2$ + H→$CH_3$ | 1.448 | 1.550 | 1.670 | 1.05 (1.05) | 0.81 (0.78) | 0.80 (0.79) |
| $CH_3$ + H→$CH_4$ | 1.436 | 1.540 | 1.551 | 1.14 (1.15) | 0.92 (0.93) | 0.88 (0.84) |

[a]Values excluding ZPE in parentheses.



DOI: 10.1021/cs501668g
ACS Catal. 2015, 5, 2203−2208

**Table 2. C−C Distances ($d_{C-C}$) at the TSs and Reaction Barriers ($E_a$), Reaction Energies ($\Delta E_r$), and Effective Barriers ($E_{eff,CHi-CHj/CO}$) of $C_1-C_1$ Coupling Reactions[a]**

| reactions | $d_{C-C}$ (Å) | $E_a$ (eV) | $\Delta E_r$ (eV) | $E_{eff,CH_i-CH_j/CO}$ (eV) |
|---|---|---|---|---|
| C + C | 1.601 | 1.55 (1.59) | 1.24 (1.23) | 1.55 (1.59) |
| C + CH | 1.778 | 1.07 (1.09) | 0.67 (0.65) | 1.66 (1.61) |
| C + $CH_2$ | 1.911 | 1.08 (1.09) | 0.24 (0.15) | 2.58 (2.46) |
| C + $CH_3$ | 2.036 | 1.23 (1.21) | 0.02 (−0.07) | 3.07 (2.81) |
| CH + CH | 1.718 | 0.96 (0.96) | 0.51 (0.43) | 1.79 (1.66) |
| CH + $CH_2$ | 1.850 | 1.03 (1.03) | 0.69 (0.64) | 2.77 (2.57) |
| CH + $CH_3$ | 2.000 | 1.44 (1.52) | 0.50 (0.42) | 3.57 (3.30) |
| $CH_2$ + $CH_2$ | 1.979 | 1.04 (0.98) | 0.00 (−0.02) | 3.66 (3.38) |
| $CH_2$ + $CH_3$ | 1.973 | 1.49 (1.45) | 0.40 (0.23) | 4.11 (3.85) |
| $CH_3$ + $CH_3$ | - | - | 0.58 (0.38) | - |
| C + CO | 1.696 | 1.66 (1.72) | 1.20 (1.24) | 1.66 (1.72) |
| CH + CO | 1.772 | 1.13 (1.13) | 0.97 (0.93) | 1.72 (1.65) |
| $CH_2$ + CO | 1.864 | 1.16 (1.14) | 0.36 (022) | 2.66 (2.51) |
| $CH_3$ + CO | 1.956 | 1.35 (1.33) | 0.30 (0.27) | 3.24 (2.93) |

[a]Values excluding ZPE in parentheses.

reactions, which would be most likely to occur on the $\chi$-$Fe_5C_2$ (510) surface under typical FTS conditions.

Aside from the carbide mechanism, the CO rather than less unstable HCO or COH[23] insertion mechanism for $C_1-C_1$ coupling reactions was also considered. The derivation details of the effective barrier of $CH_i$ + CO ($E_{eff,CH_i-CO}$) are shown in Supporting Information. The corresponding structural and energy results are also given in Figure S4 and Table 2. It can be seen that the C + CO coupling reaction has the largest reaction barrier, and the CH + CO coupling reaction has relatively lower individual reaction barrier and effective barrier than $CH_2$ +CO and $CH_3$ + CO coupling reactions. Moreover, the CH + CO coupling reaction has similar individual reaction barrier and effective barrier compared to the C + CH and CH + CH coupling reactions, which might also occur on the $\chi$-$Fe_5C_2$ (510) surface. Along this line, the CH + CO → CCH + O reaction pathways in light of carbide or CO insertion mechanism were further studied. As shown in Figure 4, the overall barrier of the CO insertion pathway is 1.56 eV, which is 0.47 eV higher than that of the carbide pathway. This indicates that the carbide mechanism is the dominating $C_1-C_1$ coupling reaction mechanism on the $\chi$-$Fe_5C_2$ (510) surface. Moreover, previous study showed that CO insertion mechanism is the favorable $C_1-C_1$ coupling mechanism on $\chi$-$Fe_5C_2$ (001) surface.[24] This indicates that $C_1-C_1$ coupling mechanism is highly sensitive to $\chi$-$Fe_5C_2$ crystal facet.

The above results show that the $C_1-C_1$ coupling reactions on the terraced-like $\chi$-$Fe_5C_2$ (510) surface mainly proceed by the C + CH and CH + CH in terms of the carbide mechanism. This is in good agreement with the steady-state isotopic transient kinetic analysis (SSITKA) results of Govender et al., i.e., both C and CH as active $C_1$ species participating in chain initiation to form reactive $C_2$ species such as CCH during high-temperature FTS on the Fe-based catalyst.[44,45] Moreover, the $C_1-C_1$ coupling reactions on the terraced-like $\chi$-$Fe_5C_2$ (510) surface were compared to those on the stepped-like $\chi$-$Fe_5C_2$ (100) surface[17] for understanding the relationship between the favorable coupling reaction and the $\chi$-$Fe_5C_2$ crystal facet, although different computational methods were employed. As shown in Figure 5, on the terraced-like surface, the coupling reaction involving relatively stable species has a lower effective barrier, and the C + CH and CH + CH are the preferred $C_1-$

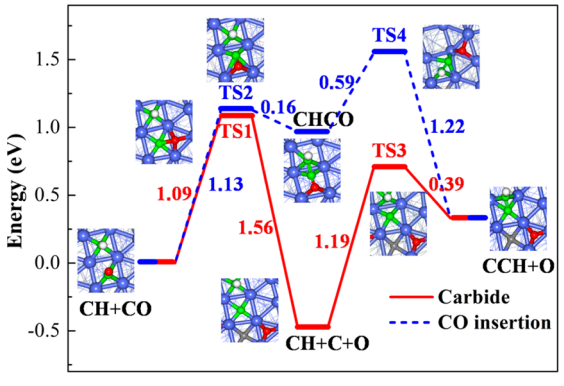


**Figure 4.** Energies and structures for the CH + CO → CCH + O formation pathways on $\chi$-$Fe_5C_2$ (510) surface in terms of the carbide mechanism (red-solid line) and CO-insertion mechanism (blue-dash line). Zero-point energies are included. Blue: Fe atoms; gray: C atoms; green: C atoms involved in reactions; white: H atoms; red: O atoms.

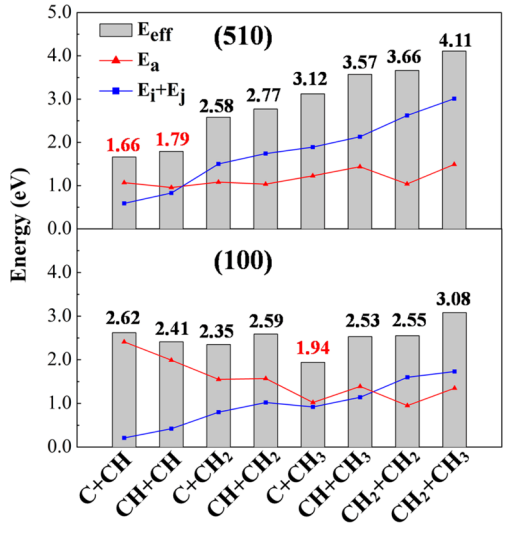


**Figure 5.** Effective barriers ($E_{eff,C-C}$) and reaction barriers ($E_a$) of $C_1-C_1$ coupling reactions and the involving reactants energies ($E_i + E_j$) on $\chi$-$Fe_5C_2$ (510) and $\chi$-$Fe_5C_2$ (100) surfaces. The data of $\chi$-$Fe_5C_2$ (100) surface are from ref 17.



DOI: 10.1021/cs501668g
ACS Catal. 2015, 5, 2203−2208

$C_1$ coupling pathways. However, on the stepped-like surface, the C + $CH_j$ coupling reaction involving relatively unstable species (e.g., C + $CH_3$) has a lower effective barrier; other $C_1$−$C_1$ coupling reactions except $CH_2$ + $CH_3$ have similar effective barriers, and the C + $CH_3$ is the preferred $C_1$−$C_1$ coupling pathways. In addition, the reaction barrier on the terraced-like surface is insensitive to the stability of reactants though the $C_1$−$C_1$ coupling reactions involving unstable $CH_3$ species have a slightly higher barrier. In contrast, the reaction barrier on the stepped-like surface is highly sensitive to the stability of reactants: the higher reaction barrier apparently arises from the more stable reactants. This would provide an interpretation for a different trend of the effective barriers and thus the preferred $C_1$−$C_1$ coupling reactions between the two surfaces. It is noted to mention that C and CH species prefer to adsorb at 4-fold sites of metal surfaces;[26,39] for the TSs structures, C and CH species adsorb at the 4-fold hollow site on $\chi$-$Fe_5C_2$ (510) surface (Figure S4); however, C species adsorb at the 3-fold site, and CH species adsorb at 2-fold or 3-fold sites on the $\chi$-$Fe_5C_2$ (100) surface.[17] It could be deduced that the difference in the active sites' structures on the two surfaces mainly contributes to the difference in the favorable $C_1$−$C_1$ coupling pathways.

**3.3. Selectivity between $CH_4$ and $C_{2+}$.** To quantify the selectivity between $CH_4$ and $C_{2+}$, the effective barrier difference between $CH_4$ formation and $C_1$−$C_1$ coupling ($\Delta E_{eff}$, the derivation details in Supporting Information[17,20]) was used a descriptor. In principle, the higher $\Delta E_{eff}$ represents the higher selectivity of $C_{2+}$ and the lower selectivity of $CH_4$. Table 3 gives a comparison of $\Delta E_{eff}$ between the $\chi$-$Fe_5C_2$ (510) surface and the reported FTS catalysts surfaces taken from the literature.[17,20,39,43] Although different computational methods were employed between our work and those reported in the literature, the comparison of the $\Delta E_{eff}$ values, not the absolute $E_{eff,CH4}$ and $E_{eff,C1-C1}$ values, is still reasonable to understand the trend of FTS selectivity. Obviously, the $\chi$-$Fe_5C_2$ (510) surface exhibits the highest $\Delta E_{eff}$ and thus the lowest selectivity of $CH_4$ as well as the highest selectivity of $C_{2+}$.

**Table 3. Effective Barriers of $CH_4$ Formation and $C_1$−$C_1$ Coupling and Their Barrier Differences on Rh, Ru, Co, Fe, and Their Carbide Surfaces**

| surface | $E_{eff,CH4}$ (eV) | $E_{eff,C1-C1}$ (eV) | $\Delta E_{eff}$ (eV) | ref |
|---|---|---|---|---|
| stepped $Co_2C$ (001) | 1.27 | 2.59 | −1.32 | 17 |
| Rh (211) | 1.23 | 1.68 | −0.45 | 20 |
| stepped Co (0001) | 1.31 | 1.55 | −0.24 | 17 |
| Fe (210) | 2.13 | 2.19 | −0.06 | 20 |
| $\chi$-$Fe_5C_2$ (100) | 1.89 | 1.94 | −0.05 | 17 |
| stepped Ru (0001) | 1.44 | 1.34 | 0.10 | 20 |
| Fe (100) | 2.13 | 1.92 | 0.21 | 39, 43 |
| $\chi$-$Fe_5C_2$ (510) | 2.39 | 1.66 | 0.73 | this work |

Considering that the real $\chi$-$Fe_5C_2$ catalyst consists of different crystal facets, probing the FTS mechanism on different $\chi$-$Fe_5C_2$ crystal facets is informative and would provide a catalyst design principle for the upgrade of FTS products with various end-use applications (e.g., transportation fuels and lower olefins). It is demonstrated that the terraced-like (510) surface prefers the direct CO dissociation[23] and the occurrence of C−C coupling reactions in terms of the carbide mechanism. However, the stepped-like (010), (001) surfaces prefer the H-assisted CO dissociation,[16,24] and the (100) surface prefers both direct and H-assisted CO dissociation;[25] both exhibit different FTS behaviors.[16,17,25,46] Moreover, the $CH_4$ formation effective barrier of the (010) surface[16] is 1.54 eV, which is much lower than that of the (510) surface (i.e., 2.39 eV). This suggests that the step sites of $\chi$-$Fe_5C_2$ catalyst are more active toward $CH_4$ formation, which is consistent with the experimental results of de Jong and co-workers.[47] All of these results revealed that manipulating the crystal facets of $\chi$-$Fe_5C_2$ catalyst could be an effective method to tune FTS selectivity, which would shed new light on preparing highly selective $\chi$-$Fe_5C_2$ FTS catalyst by the well-defined preparation method. However, it is worth mentioning that there is still plenty of room for understanding the FTS mechanism on the $\chi$-$Fe_5C_2$ catalyst, owing to wide product distribution (e.g., paraffins, olefins, and oxygenates present in minor amounts)[19] and thus involving various surface intermediates and elementary steps. Up to now, a direct relationship between the $\chi$-$Fe_5C_2$ crystal facet and FTS selectivity is still unclear, and we will investigate this relationship in our future work.

## CONCLUSIONS

In summary, we theoretically identify that for FTS on a thermodynamically stable, terraced-like $\chi$-$Fe_5C_2$ (510) surface, the surface C-occupied site is inactive toward $CH_4$ formation; all the three cases exhibit high effective barriers of $CH_4$ formation (i.e., 3.66, 2.81, and 2.39 eV), indicating the unfavorable occurrence of $CH_4$ formation under the FTS condition. The C + CH and CH + CH are the most likely coupling pathways in terms of the carbide mechanism. $CH_4$ formation and $C_1$−$C_1$ coupling mechanisms are highly sensitive to the $\chi$-$Fe_5C_2$ crystal facet. Moreover, FTS selectivity between this surface and the reported FTS catalysts' surfaces are compared and discussed in detail. This surface shows unexpectedly high $C_{2+}$ selectivity. This strongly indicates that manipulating the crystal facets of the $\chi$-$Fe_5C_2$ catalyst would effectively tune FTS selectivity. The insights revealed here will guide the design and optimization of highly selective $\chi$-$Fe_5C_2$ FTS catalysts.

## ASSOCIATED CONTENT

### Supporting Information

The following file is available free of charge on the ACS Publications website at DOI: 10.1021/cs501668g.

Derivations of effective barriers of $CH_4$ formation and $C_1$−$C_1$ coupling and their barrier difference, Tables S1−S3 and Figures S1−S4 (PDF)

## AUTHOR INFORMATION

### Corresponding Author

*E-mail: xzduan@ecust.edu.cn. Fax: +86-21-64253528.

### Notes

The authors declare no competing financial interest.

## ACKNOWLEDGMENTS

This work is financially supported by the Natural Science Foundation of China (21306046) and the 111 Project of Ministry of Education of China (B08021).

## REFERENCES

(1) Khodakov, A. Y.; Chu, W.; Fongarland, P. *Chem. Rev.* **2007**, *107*, 1692−1744.



DOI: 10.1021/cs501668g
*ACS Catal.* 2015, 5, 2203−2208

(2) Tijmensen, M. J. A.; Faaij, A. P. C.; Hamelinck, C. N.; van Hardeveld, M. R. M. *Biomass Bioenerg.* **2002**, *23*, 129−152.
(3) de Klerk, A. *Energy Environ. Sci.* **2011**, *4*, 1177−1205.
(4) Abello, S.; Montane, D. *ChemSusChem* **2011**, *4*, 1538−1556.
(5) Torres Galvis, H. M.; de Jong, K. P. *ACS Catal.* **2013**, *3*, 2130−2149.
(6) Liu, Y. F.; Ersen, O.; Meny, C.; Luck, F.; Pham-Huu, C. *ChemSusChem* **2014**, *7*, 1218−1239.
(7) van der Laan, G. P.; Beenackers, A. A. C. M. *Catal. Rev. Sci. Eng.* **1999**, *41*, 255−318.
(8) Iglesia, E. *Appl. Catal., A* **1997**, *161*, 59−78.
(9) Dry, M. E. *Catal. Today* **2002**, *71*, 227−241.
(10) Schulz, H. *Appl. Catal., A* **1999**, *186*, 3−12.
(11) Biloen, P.; Sachtler, W. M. H. *Adv. Catal.* **1981**, *30*, 165−216.
(12) Yang, J.; Ma, W. P.; Chen, D.; Holmen, A.; Davis, B. H. *Appl. Catal., A* **2014**, *470*, 250−260.
(13) Torres Galvis, H. M.; Koeken, A. C. J.; Bitter, J. H.; Davidian, T.; Ruitenbeek, M.; Dugulan, A. I.; de Jong, K. P. *J. Catal.* **2013**, *303*, 22−30.
(14) Steynberg, A.; Dry, M. E. In *Stud. Surf. Sci. Catal.*; Elsevier: Amsterdam, 2004; Vol. *152*, p 196.
(15) Herranz, T.; Rojas, S.; Perez-Alonso, F. J.; Ojeda, M.; Terreros, P.; Fierro, J. L. G. *J. Catal.* **2006**, *243*, 199−211.
(16) Huo, C. F.; Li, Y. W.; Wang, J. G.; Jiao, H. J. *J. Am. Chem. Soc.* **2009**, *131*, 14713−14721.
(17) Cheng, J.; Hu, P.; Ellis, P.; French, S.; Kelly, G.; Lok, C. M. *J. Phys. Chem. C* **2010**, *114*, 1085−1093.
(18) de Smit, E.; Cinquini, F.; Beale, A. M.; Safonova, O. V.; van Beek, W.; Sautet, P.; Weckhuysen, B. M. *J. Am. Chem. Soc.* **2010**, *132*, 14928−14941.
(19) Yang, C.; Zhao, H. B.; Hou, Y. L.; Ma, D. *J. Am. Chem. Soc.* **2012**, *134*, 15814−15821.
(20) Cheng, J.; Hu, P.; Ellis, P.; French, S.; Kelly, G.; Lok, C. M. *J. Phys. Chem. C* **2009**, *113*, 8858−8863.
(21) Retief, J. J. *Powder Diffr.* **1999**, *14*, 130−132.
(22) Huang, G. M.; Hu, J.; Zhang, H.; Zhou, Z. J.; Chi, X. Q.; Gao, J. H. *Nanoscale* **2014**, *6*, 726−730.
(23) Pham, T. H.; Duan, X. Z.; Qian, G.; Zhou, X. G.; Chen, D. *J. Phys. Chem. C* **2014**, *118*, 10170−10176.
(24) Cao, D. B.; Li, Y. W.; Wang, J. G.; Jiao, H. J. *J. Mol. Catal. A: Chem.* **2011**, *346*, 55−69.
(25) Ozbek, M. O.; Niemantsverdriet, J. W. *J. Catal.* **2014**, *317*, 158−166.
(26) Liu, J. X.; Su, H. Y.; Sun, D. P.; Zhang, B. Y.; Li, W. X. *J. Am. Chem. Soc.* **2013**, *135*, 16284−16287.
(27) Kresse, G.; Hafner, J. *Phys. Rev. B* **1993**, *47*, 558−561.
(28) Kresse, G.; Hafner, J. *Phys. Rev. B* **1994**, *49*, 14251−14269.
(29) Kresse, G.; Furthmuller, J. *Comput. Mater. Sci.* **1996**, *6*, 15−50.
(30) Kresse, G.; Furthmuller, J. *Phys. Rev. B* **1996**, *54*, 11169−11186.
(31) Blochl, P. E. *Phys. Rev. B* **1994**, *50*, 17953−17979.
(32) Kresse, G.; Joubert, D. *Phys. Rev. B* **1999**, *59*, 1758−1775.
(33) Perdew, J. P.; Burkem, K.; Ernzerhof, M. *Phys. Rev. Lett.* **1996**, *77*, 3865−3868.
(34) Monkhorst, H. J.; Pack, J. D. *Phys. Rev. B* **1976**, *13*, 5188−5192.
(35) Methfessel, M.; Paxton, A. T. *Phys. Rev. B* **1989**, *40*, 3616−3621.
(36) Henkelman, G.; Jonsson, H. *J. Chem. Phys.* **1999**, *111*, 7010−7022.
(37) Sheppard, D.; Terrell, R.; Henkelman, G. *J. Chem. Phys.* **2008**, *128*, 134106.
(38) Lo, J. M. H.; Ziegler, T. *J. Phys. Chem. C* **2007**, *111*, 11012−11025.
(39) Govender, A.; Ferre, D. C.; Niemantsverdriet, J. W. *ChemPhysChem* **2012**, *13*, 1591−1596.
(40) Storsæter, S.; Chen, D.; Holmen, A. *Surf. Sci.* **2006**, *600*, 2051−2063.
(41) Cheng, J.; Gong, X. Q.; Hu, P.; Lok, C. M.; Ellis, P.; French, S. *J. Catal.* **2008**, *254*, 285−295.
(42) Lo, J. M. H.; Ziegler, T. *J. Phys. Chem. C* **2007**, *111*, 13149−13162.
(43) Govender, A.; Curulla-Ferre, D.; Perez-Jigato, M.; Niemantsverdriet, J. W. *Molecules* **2013**, *18*, 3806−3824.
(44) Govender, N. S.; Botes, F. G.; de Croon, M. H. J. M.; Schouten, J. C. *J. Catal.* **2008**, *260*, 254−261.
(45) Govender, N. S.; Botes, F. G.; de Croon, M. H. J. M.; Schouten, J. C. *J. Catal.* **2014**, *312*, 98−107.
(46) Cao, D. B.; Li, Y. W.; Wang, J. G.; Jiao, H. J. *J. Phys. Chem. C* **2008**, *112*, 14883−14890.
(47) Torres Galvis, H. M.; Bitter, J. H.; Davidian, T.; Ruitenbeek, M.; Dugulan, A. I.; de Jong, K. P. *J. Am. Chem. Soc.* **2012**, *134*, 16207−16215.


DOI: 10.1021/cs501668g
*ACS Catal.* 2015, 5, 2203−2208